World Academy of Science, Engineering and Technology
International Journal of Aerospace and Mechanical Engineering
Vol:8, No:7, 2014

# Material Failure Process Simulation by Improve Finite Elements with Embedded Discontinuities

Juárez-Luna Gelacio, Ayala Gustavo, Retama-Velasco Jaime



***Abstract*—**This paper shows the advantages of the material failure process simulation by improve finite elements with embedded discontinuities, using a new definition of traction vector, dependent on the discontinuity length and the angle. Particularly, two families of this kind of elements are compared: kinematically optimal symmetric and statically and kinematically optimal non-symmetric. The constitutive model to describe the behavior of the material in the symmetric formulation is a traction-displacement jump relationship equipped with softening after reaching the failure surface.

To show the validity of this symmetric formulation, representative numerical examples illustrating the performance of the proposed formulation are presented. It is shown that the non-symmetric family may over or underestimate the energy required to create a discontinuity, as this effect is related with the total length of the discontinuity, fact that is not noticed when the discontinuity path is a straight line.

***Keywords*—**Variational formulation, strong discontinuity, embedded discontinuities, strain localization.

## I. Introduction

THE idea of lumping a strain concentration into a line or surface for 2D and 3D quasi-static damage mechanics problems, respectively, has motivated the development and application of solid finite elements with embedded discontinuities (FEEDs) [2], [8]-[14], [26], [28], [29], [30]. An extension of this technique was the development of finite elements simulating hinges in beams [3], [5], [15] and [16] and an extended formulation for the analysis of softening hinge lines in inelastic thick plates [6]. More recently, FEEDs have been used for dynamic fracture simulations [3], [4] and [17]. In the formulation of these kinds of elements, there are mainly two requirements which must be satisfied in the localization zone: 1) equilibrium, traction continuity across the discontinuity interface and 2) kinematics, free relative rigid body motions of the two portions of an element split up by a discontinuity.

A comprehensive study of FEEDs is found in [18], where these elements are classified into three families: 1) statically optimal symmetric (SOS), which satisfies equilibrium but does not kinematics; 2) kinematically optimal symmetric (KOS), which satisfies kinematics and apparently does not satisfy equilibrium; and 3) statically and kinematically optimal non-symmetric (SKON), which satisfies both equilibrium and kinematics. New symmetric FEEDs, including mixed and assumed enhanced strain techniques, have been explored by [24], showing that although these symmetric FEEDs reduced the stress locking problem, the SKON formulations still provide better results. Recently, [20] have shown that KOS formulations satisfies both equilibrium and kinematics, introducing a new definition of the traction vector, which is dependent on the discontinuity length and on the direction; with this formulation, the energy necessary to create a discontinuity is coherent with its length.

This paper shows the advantages of the material failure process simulation with FEEDs developed by [20] from the KOS family. The equilibrium in the KOS formulation is satisfied by a new definition of traction as a function of the length of the discontinuity, in the sense that the two equations at the residual are forces.

The outline of this paper is as follows. Section II provides the equations defining kinematics and the boundary value problem (BVP) of a solid with discontinuities and the discrete constitutive model to describe the behavior of the material in for the development of discontinuities. Section III presents the energy functional of solids with strong discontinuities for the KOS formulation. Section IV shows the finite element approximation of the variational formulation with strong discontinuities. Numerical examples of elements with discontinuities, which validate the proposed formulation, are presented in Section V. Finally, in Section VI, conclusions derived from the work are given.

## II. Problem Definition

### A. Boundary Value Problem

Consider a 3D body, defined by an open bounded domain, $\Omega \in \mathrm{R}^3$, and boundary, $\Gamma$, (Fig. 1a), loaded until it undergoes a displacement discontinuity, $[|\mathbf{u}|]$, across a surface, $S$, where the inelastic deformations are concentrated. This discontinuity splits the domain into two sub-domains such that, $\Omega = \Omega^- + \Omega^+ + S$, with two boundaries, $\Gamma = \Gamma^- + \Gamma^+$. The boundary conditions are the prescribed surface tractions, $\mathbf{t}^*$, on $\Gamma_\sigma = \Gamma_\sigma^- + \Gamma_\sigma^+$ and the prescribed displacements, $\mathbf{u}^*$, on $\Gamma_u = \Gamma_u^- + \Gamma_u^+$, such that $\Gamma_\sigma \cup \Gamma_u = \Gamma$ and $\Gamma_\sigma \cap \Gamma_u = \varnothing$. This problem may be idealized using two different approaches: Strong Discontinuity (SD) and Discrete Discontinuity (DD). The first approach considers that $\Omega$ remains continuous after $[|\mathbf{u}|]$ initiates (Fig. 1b), with a

G. Juárez-Luna is with Materials Department, Universidad Autónoma Metropolitana, San Pablo 180, Col. Reynosa Tamaulipas, Azcapotzalco, CO 02200 Mexico City (phone: 5255-5318-9085; fax: 5255-5318-9085; e-mail: gjl@azc.uam.mx).

G. Ayala and J. Retama-Velazco are with Applied Mechanics, Universidad Nacional Autónoma de México, Ciudad Universitaria 3000, Coyoacán, CO 04510 Mexico City (phone: 5255-5623-3508; fax: 5255-5623-3508; e-mail: gayalam@ ii.unam.mx, jretamav@ii.unam.mx).

material behavior described by non-linear stress-strain constitutive equations. The second approach considers that Ω stops being continuous, due to the development of *S* (Fig. 1c) and that, there is traction transmission, related with[|**u**|], throughout the discontinuity borders. Consequently, the constitutive behavior of the material around the discontinuity is described by traction-separation constitutive laws, whereas the rest of the domain, $\Omega / S = \Omega^+ + \Omega^-$, is described by standard constitutive laws.

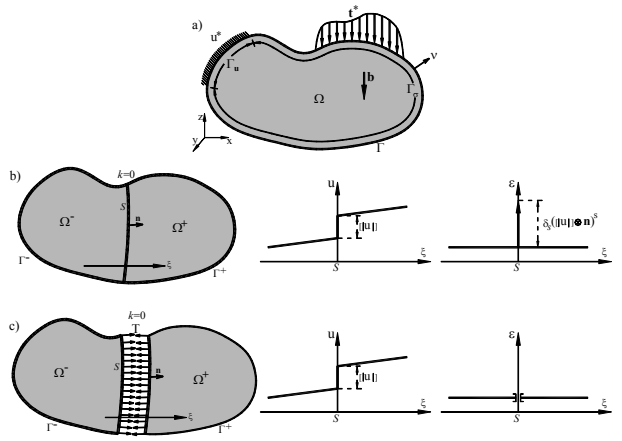


Fig. 1 Continuum Ω with: (a) boundary conditions, (b) SD and (c) DD

The discontinuous displacement field**u**, with a jump [|**u**|]at a given (material) point*S*, induces an unbounded strain field. Both fields can be expressed as:

$$\begin{aligned} \mathbf{u} &= \bar{\mathbf{u}} + H_S(\mathbf{x})[|\mathbf{u}|](\mathbf{x},t) \\ \boldsymbol{\varepsilon} &= \nabla^S \mathbf{u} = \bar{\boldsymbol{\varepsilon}} + \delta_s([|\mathbf{u}|]\otimes\mathbf{n})^S \end{aligned} \tag{1}$$

where $\bar{\mathbf{u}}$ is the continuous part of the displacements and $\bar{\boldsymbol{\varepsilon}}$ the continuous part of the strains, $H_S$ is the Heaviside function defined on *S* ($H_s(\mathbf{x})=0\ \forall \mathbf{x}\in\Omega^-$ y $H_s(\mathbf{x})=1\ \forall \mathbf{x}\in\Omega^+$), and $\delta_S$ is the Dirac delta function.

The BVP for SD and DD formulations is defined by the next equations and boundary conditions:

| | | | |
|---|---|---|---|
| *a*) | Kinematical compatibility | $\bar{\boldsymbol{\varepsilon}}^{\mathbf{u}} - \bar{\boldsymbol{\varepsilon}} = 0$ | in $\Omega / S$ |
| *b*) | Constitutive compatibility | $\boldsymbol{\sigma}^{\bar{\boldsymbol{\varepsilon}}} - \boldsymbol{\sigma} = \mathbf{0}$ | in $\Omega / S$ |
| *c*) | Internal equilibrium | $\nabla\cdot\boldsymbol{\sigma} + \mathbf{b} = \mathbf{0}$ | in $\Omega / S$ |
| *d*) | External equilibrium | $\boldsymbol{\sigma}\cdot\boldsymbol{\nu} = \mathbf{t}^*$ | on $\Gamma_\sigma$ |
| | | $\boldsymbol{\sigma}\cdot\boldsymbol{\nu} = \mathbf{t}$ | on $\Gamma_u$ |
| *e*) | Essential boundary condition | $\mathbf{u} = \mathbf{u}^*$ | on $\Gamma_u$ |
| *f*) | Inner traction continuity | $\boldsymbol{\sigma}_{\Omega^-}\cdot\mathbf{n} - \underbrace{\boldsymbol{\sigma}_S\cdot\mathbf{n}}_{\mathbf{T}} = \mathbf{0}$ | on *S* |
| | | $\boldsymbol{\sigma}_{\Omega^+}\cdot\mathbf{n} - \underbrace{\boldsymbol{\sigma}_S\cdot\mathbf{n}}_{\mathbf{T}} = \mathbf{0}$ | |
| *g*) | Outer traction continuity | $\underbrace{\boldsymbol{\sigma}_{\Omega^+}\cdot\mathbf{n} - \boldsymbol{\sigma}_{\Omega^-}\cdot\mathbf{n}}_{[|\boldsymbol{\sigma}|]_{\Omega/S}\cdot\mathbf{n}} = \mathbf{0}$ | on *S* |

(2)

In the SD formulation, the tractions, given in (2), are computed from the projected stresses $\boldsymbol{\sigma}_S$, from a stress-strain constitutive law, whereas in the DD, these tractions are computed directly from a traction-displacement relationship.

*B. Constitutive Discrete Damage Model*

The isotropic discrete damage model, shown in Fig. 2, is defined by [23]as:

| | |
|---|---|
| Discrete free energy density | $\phi([|\mathbf{u}|],\bar{\alpha}) = (1-\omega)\phi_0(\bar{\alpha}),\ \begin{cases}\phi_0([|\mathbf{u}|]) = \frac{1}{2}[|\mathbf{u}|]\cdot\mathbf{Q}^{\mathbf{e}}\cdot[|\mathbf{u}|] \\ \mathbf{Q}^{\mathbf{e}} = \mathbf{n}\cdot\mathbf{C}\cdot\mathbf{n}\end{cases}$ |
| Constitutive equation | $\mathbf{T} = \frac{\partial\phi([|\mathbf{u}|],\bar{\alpha})}{\partial[|\mathbf{u}|]} = (1-\omega)\mathbf{Q}^{\mathbf{e}}\cdot[|\mathbf{u}|]$ |
| Damage variable | $\omega = 1 - \frac{\bar{q}(\bar{\alpha})}{\bar{\alpha}};\ \ \omega\in[-\infty,1]$ |
| Evolution law | $\dot{\bar{\alpha}} = \dot{\bar{\lambda}} = \frac{\partial}{\partial t}(\bar{\alpha}),\ \ \bar{\alpha}\in[0,\infty]$ |
| Damage criterion | $f(\mathbf{T},\bar{q}) = \tau_{\mathbf{T}} - \bar{q};\ \ \tau_{\mathbf{T}} = \|\mathbf{T}\|_{\mathbf{Q}^{e-1}} = \sqrt{\mathbf{T}\cdot\mathbf{Q}^{e-1}\cdot\mathbf{T}}$ |
| Hardening rule | $\dot{\bar{q}}(\bar{\alpha}) = \bar{H}\dot{\bar{\alpha}};\ \ \bar{H} = \bar{q}'(\bar{\alpha}) \le 0$ |
| Loading-unloading conditions | $f\le 0;\ \ \dot{\bar{\lambda}}\ge 0;\ \ \dot{\bar{\lambda}} f = 0;\ \ \dot{\bar{\lambda}}\dot{f} = 0$ (consistency) |

(3)

where $\phi$ is the discrete free energy density, *T* is the traction vector. The damage variable ω is defined in terms of the hardening/softening variable $\dot{\bar{q}}$, which is dependent on the hardening/softening parameter $\bar{H}$. The damage multiplier $\dot{\bar{\lambda}}$ determines the loading-unloading conditions, the function $f(\mathbf{T},\bar{q})$, bounds the elastic domain defining the damage surface in the tractions space.

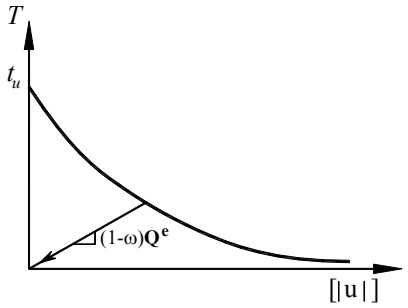


Fig. 2 Discrete damage model

The tangent constitutive equation, in terms of rates from the model in (3) is:

$$\dot{\mathbf{T}} = \mathbf{C}_d^T\cdot[|\dot{\mathbf{u}}|] \tag{4}$$

where $\mathbf{C}_d^T$ is the discrete tangent constitutive operator, relating the traction and the jump displacement of the nonlinear loading range, which is defined by

$$\mathbf{C}_d^T = (1-\omega)\mathbf{Q}^{\mathbf{e}} - \frac{\bar{q}-\bar{H}\bar{\alpha}}{\bar{\alpha}^3}\left(\mathbf{Q}^{\mathbf{e}}\cdot[|\mathbf{u}|]\otimes[|\mathbf{u}|]\cdot\mathbf{Q}^{\mathbf{e}}\right) \tag{5}$$

and for the elastic loading and unloading range ( $\dot{\omega} = 0$ ):

$$\mathbf{C}_d^T = (1-\omega)\mathbf{Q}^{\mathbf{e}} \tag{6}$$

## III. Variational Formulation

### A. Symmetric Formulations

The KOS approximation is based on the displacement functional [1], [19]-[21] and [31]:

$$\Pi(\mathbf{u},[|\mathbf{u}|]) = \int_{\Omega/S}\left[\Psi(\bar{\boldsymbol{\varepsilon}}^u) - \mathbf{b}\cdot\mathbf{u}\right]d\Omega - \int_{\Gamma_\sigma}\mathbf{t}^*\cdot\mathbf{u}d\Gamma + \int_{\Gamma_S}\phi_S([|\mathbf{u}|])d\Gamma \tag{7}$$

where the free energy density $\Psi(\bar{\boldsymbol{\varepsilon}}^u)$ ,depends on the continuous strain field $\bar{\boldsymbol{\varepsilon}}$ , and the free discrete energy density, $\Psi_S([|\mathbf{u}|])$ depends on the jump given by:

$$\Psi(\bar{\boldsymbol{\varepsilon}}) = \int_0^{\bar{\boldsymbol{\varepsilon}}}\boldsymbol{\sigma}(\bar{\boldsymbol{\varepsilon}})\,d\bar{\boldsymbol{\varepsilon}}$$
$$\phi_S([|\mathbf{u}|]) = \int_0^{[|\mathbf{u}|]}\mathbf{T}_S([|\mathbf{u}|]_{n,s})\,d[|\mathbf{u}|] \tag{8}$$

From which the elastic stress$\boldsymbol{\sigma}$, is defined by:

$$\boldsymbol{\sigma} = \mathbf{C} : \bar{\boldsymbol{\varepsilon}} \tag{9}$$

The first variation of the functional given in (7) is:

$$\delta\Pi = -\int_{\Omega/S}(\nabla\cdot\boldsymbol{\sigma}+\mathbf{b})\cdot\delta\mathbf{u}d\Omega + \int_{\Gamma_\sigma}\left(\boldsymbol{\sigma}\cdot\boldsymbol{\nu}-\mathbf{t}^*\right)\cdot\delta\mathbf{u}d\Gamma + \int_{\Gamma_u}\left(\boldsymbol{\sigma}^{\boldsymbol{\varepsilon}}\cdot\boldsymbol{\nu}-\mathbf{t}\right)\cdot\delta\mathbf{u}\,d\Gamma + \int_S\mathbf{n}\cdot(\boldsymbol{\sigma}_{\Omega^+}-\boldsymbol{\sigma}_{\Omega^-})\cdot\delta\mathbf{u}\,d\Gamma - \int_{\Gamma_S}\left(\boldsymbol{\sigma}\cdot\mathbf{n}-\mathbf{C}_d^T:[|\mathbf{u}|]_{n,s}\right)d\Gamma \tag{10}$$

which unlike non-symmetric formulation, it also includes the inner traction continuity of the BVP.

## IV. Finite Element Approximation

### A. Discretization

1) Regularization of the Displacement Kinematics

It is not possible to prescribe the boundary conditions, $\mathbf{u}^*$, in only one of the displacement fields, $\bar{\mathbf{u}}$ or$[|\mathbf{u}|]$, this difficulty is overcome, according to [22], by defining the displacement field as in (11), see Fig. 3a and b, *i.e.*,

$$\mathbf{u} = \hat{\mathbf{u}} + M_S(\mathbf{x})[|\mathbf{u}|]_{x,y} \tag{11}$$

Then, the strain field is defined by:

$$\boldsymbol{\varepsilon} = \nabla^S\mathbf{u} = \nabla^S\hat{\mathbf{u}} + \nabla^S M_S(\mathbf{x})[|\mathbf{u}|]_{x,y} \tag{12}$$

where $\hat{\mathbf{u}}$ is the regular displacement field and $M_s(\mathbf{x})$ is a function given by:

$$M_S(\mathbf{x}) = H_S(\mathbf{x}) - \phi(\mathbf{x}) \tag{13}$$

where $\phi(\mathbf{x})$is a continuous function such that:

$$\phi(\mathbf{x}) = 0 \ \ \forall\mathbf{x}\in\Omega^-$$
$$\phi(\mathbf{x}) = 1 \ \ \forall\mathbf{x}\in\Omega^+ \tag{14}$$

The function $M_S$, has two properties: $M_S(x) = 1 \ \ \forall x \in S$ and $M_S(x) = 0 \ \ \forall x \in \Omega^- \cup \Omega^+$ (Fig. 3c).

The continuous displacement field of (1) is now defined as:

$$\bar{\mathbf{u}} = \hat{\mathbf{u}} - \phi(\mathbf{x})[|\mathbf{u}|]_{x,y} \tag{15}$$

In the continuous part of the solid, which may be linear elastic, the continuous strain field, $\bar{\boldsymbol{\varepsilon}}$is given by:

$$\bar{\boldsymbol{\varepsilon}} = \nabla^S\bar{\mathbf{u}} \tag{16}$$

Substituting (15) into (16),

$$\bar{\boldsymbol{\varepsilon}} = \nabla^S\hat{\mathbf{u}} - \nabla^S\phi(\mathbf{x})[|\mathbf{u}|]_{x,y} - \phi(\mathbf{x})\nabla^S[|\mathbf{u}|]_{x,y} \tag{17}$$

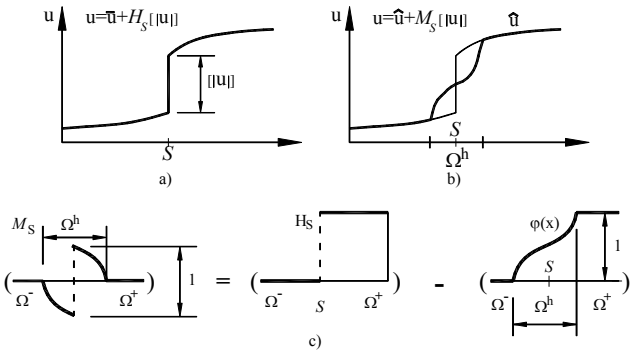


Fig. 3 Graphic representation of: (a) continuous displacements, (b) regular displacements and (c) function $M_S$.

If the displacement jump is constant in(17), the continuous strain field may be rewritten as:

$$\bar{\boldsymbol{\varepsilon}} = \nabla^S\hat{\mathbf{u}} - \nabla^S\phi(\mathbf{x})[|\mathbf{u}|]_{x,y} \tag{18}$$

For 2D problems, the displacement jump and traction vector are defined in a local system *n,s* or in a global system *x,y* as shown in Fig. 4.

$$[|\mathbf{u}|]_{n,s} = \mathbf{R}[|\mathbf{u}|]_{x,y}$$
$$\mathbf{T}_{n,s} = \mathbf{R}\mathbf{T}_{x,y} \tag{19}$$

where $\mathbf{R}$ is defined as:

$$\mathbf{R} = \begin{bmatrix}\cos\theta & \sin\theta\\ -\sin\theta & \cos\theta\end{bmatrix} \tag{20}$$

The traction $\mathbf{T}_{x,y}$ in a global system is computed by:

$$\mathbf{T}_{x,y} = \boldsymbol{\sigma} \cdot \mathbf{n} \tag{21}$$

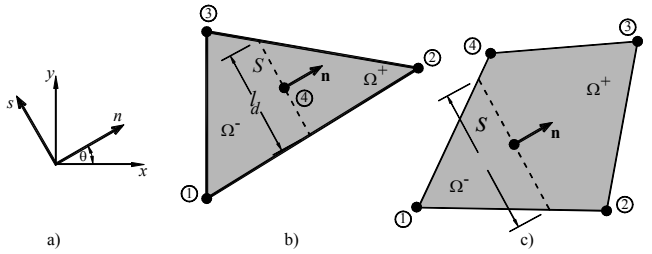


Fig. 4 Discontinuity: a) reference system, b) triangle element and c) quadrilateral element

2) Approximation of the Displacement and Strain Fields

The regular displacement field is approximated by:

$$\hat{\mathbf{u}} = \mathbf{N}\mathbf{d} \tag{22}$$

where **N** is the standard vector of shape functions of the element

$$\mathbf{N} = \sum_{i=1}^{i=n} N_i^{(e)} \tag{23}$$

and **d**, is the nodal displacement vector. The function, $M_s(\mathbf{x})$, is defined in the finite element approximation as:

$$M_S^e(\mathbf{x}) = H_S^e(\mathbf{x}) - \phi^e \tag{24}$$

where $\phi^e$ is constructed by:

$$\phi^e = \sum_{i^+=1}^{n_e^+} N_{i^+} \tag{25}$$

where $N_{i^+}$ are the shape functions corresponding to the nodes placed on $\Omega^+$ of the finite element which contains the discontinuity, in agreement with the definition of ϕ in (14).

The displacement field defined in (11) is given by

$$\mathbf{u} = \mathbf{N}\mathbf{d} + \underbrace{M_S^e}_{\mathbf{N}_c} [|\mathbf{u}|]_{x,y} \tag{26}$$

The continuous strain field in (18)is approximated as:

$$\bar{\boldsymbol{\varepsilon}} = \mathbf{B} \cdot \mathbf{d} - \underbrace{\nabla \phi^e}_{\mathbf{B}_c} \cdot [|\mathbf{u}|]_{x,y} \quad \forall \mathbf{x} \in \Omega / S \tag{27}$$

and the unbounded strain field as:

$$\tilde{\boldsymbol{\varepsilon}}^{[|\mathbf{u}|]} = \delta_s \left( \mathbf{n} \otimes [|\mathbf{u}|]_{x,y} \right) \quad \forall \mathbf{x} \in S \tag{28}$$

where **B**, is the standard strain interpolation matrix, containing the derivatives of the standard shape functions $\partial(\mathbf{Nd})=\mathbf{Bd}$.

*B. Extremization of the Energy Functional*

The equilibrium equations corresponding to this formulation are obtained by substituting (26) and (27) into the energy functional of (7), and setting the derivatives with respect to the variables (**d**and[|**u**|]) to zero,

$$\frac{\partial \Pi}{\partial \mathbf{d}} = 0 = \int_{\Omega/S} \mathbf{B}^T \boldsymbol{\sigma}(\bar{\boldsymbol{\varepsilon}}) d\Omega - \int_{\Omega} \mathbf{N}^T \cdot \mathbf{b} d\Omega - \int_{\Gamma_\sigma} \mathbf{N}^T \cdot \mathbf{t}^* d\Gamma \tag{29}$$

$$\frac{\partial \Pi}{\partial \mathbf{d}} = 0 = -\int_{\Omega/S} \mathbf{B}_c^T \boldsymbol{\sigma}(\bar{\boldsymbol{\varepsilon}}) d\Omega + \int_{\Gamma_S} \mathbf{T}_{x,y} d\Gamma \tag{30}$$

As in (29) and (30), $\boldsymbol{\sigma}(\bar{\boldsymbol{\varepsilon}})$ and $\mathbf{T}_{x,y}$ are nonlinear, their respective linearizations with Taylor series give:

$$\begin{bmatrix} \int_{\Omega/S} \mathbf{B}^{\mathbf{T}} \cdot \mathbf{C} \cdot \mathbf{B} d\Omega & -\int_{\Omega/S} \mathbf{B}^{\mathbf{T}} \cdot \mathbf{C} \cdot \mathbf{B}_c d\Omega \\ -\int_{\Omega/S} \mathbf{B}_c^{\mathbf{T}} \cdot \mathbf{C} \cdot \mathbf{B} d\Omega & -\int_{\Omega/S} \mathbf{B}_c^{\mathbf{T}} \cdot \mathbf{C} \cdot \mathbf{B}_c d\Omega + \int_{\Gamma_S} \mathbf{R}^T \cdot \mathbf{T} \cdot \mathbf{R} d\Gamma \end{bmatrix}^{(n,0)} \begin{Bmatrix} \Delta d \\ \Delta[|\mathbf{u}|]_{x,y} \end{Bmatrix}^{(n,1)} = \begin{Bmatrix} R_1 \\ R_2 \end{Bmatrix}^{(n,0)} \tag{31}$$

where $R_1$ and $R_2$ are defined as:

$$R_1 = F_{ext}^{(n)} - \int_{\Omega/S} \mathbf{B}^T \boldsymbol{\sigma}(\bar{\boldsymbol{\varepsilon}}) d\Omega^{(n,0)} \tag{32}$$

$$R_2 = \int_{\Omega/S} \mathbf{B}_c^T \boldsymbol{\sigma}(\bar{\boldsymbol{\varepsilon}}) d\Omega^{(n,0)} - \int_{\Gamma_S} \mathbf{T}_{x,y} d\Gamma^{(n,0)} \tag{33}$$

To reduce the size of the system given in (31), the additional degrees of freedom, Δ[|**u**|], may be condensed. In (32), $R_1$ means the equilibrium between the external and the internal forces in the domain Ω\S, whereas $R_2$, in (33), the equilibrium between the forces in the domain Ω\Sand forces in the discontinuity $\Gamma_S$; $R_1$and $R_2$have units of force, unlike the SKON formulation, which one equation have units of force but the other equation has units of force/length².

*C. Tractions at Discontinuity*

To consistently achieve equilibrium in the KOS formulation, the $R_2$ forces given in (33), must be enforced to zero. Then, according to [20]

$$\int_{\Gamma_S} \mathbf{T}_{x,y} d\Gamma = \int_{\Omega/S} \mathbf{B}_c^T \boldsymbol{\sigma} d\Omega \tag{34}$$

Considering that tractions at the discontinuity are constant values for this element, (34) becomes:

$$\mathbf{T}_{x,y} = \frac{1}{l_d} \int_{\Omega/S} \mathbf{B}_c^T \boldsymbol{\sigma} d\Omega \tag{35}$$

which expressed in the local system becomes

$$\mathbf{T}_{n,s} = \frac{1}{l_d} \mathbf{R} \int_{\Omega/S} \mathbf{B}_c^T \boldsymbol{\sigma} d\Omega \tag{36}$$

the definition of traction given in (35) is different to those used by [27]:

$$\mathbf{T}_{x,y} = \frac{1}{l_d}\int_l \boldsymbol{\sigma}\cdot\mathbf{n}dl = \boldsymbol{\sigma}\cdot\mathbf{n} \tag{37}$$

$$\mathbf{T}_{x,y} = \frac{1}{hl_d}\int_{\Omega/S} \boldsymbol{\sigma}\cdot\mathbf{n}^{+}d\Omega = \frac{A_e}{hl_d}\boldsymbol{\sigma}\cdot\mathbf{n}^{+} \tag{38}$$

where $A_e$ is the element area and $\mathbf{n}^{+}$ the unit normal to a border.

## V. Numerical Examples

### A. Triangle with Discontinuity Non Parallel to a Border

Fig. 5 shows a constant strain triangle with the following mechanical properties: Young´s modulus, *E=1000 MPa*, Poisson ratio υ=0.0, maximum tensile stress, $t_u$=1 *MPa* and fracture energy density $G_f$=*0.005MN/m*. From its performed elastic analysis, imposing a horizontal displacement of *d*=0.000634755 at node 2, the stresses obtained were $\sigma_x$=0.413251, $\sigma_y$=0.082650 and $\sigma_{xy}$=-0.198361. With these stresses, the major principal stress direction is $\theta$=*-25.097°* . After this, the nonlinear analyses of this element with three different locations of the discontinuity with direction perpendicular to the major principal stress direction were carried out. The locations of the considered discontinuities with lengths: $l_{d1}$=*0.179*, $l_{d2}$=*0.358*and$l_{d3}$=*0.534*, are shown in Fig. 5b to d. In this example, the discontinuities are not parallel to a border of the element.

The load *Pvs.* displacement *d* curves for each discontinuity are shown in Fig. 6, these cases do not show numerical problems when $t_n$ reaches the maximum tensile traction. Nevertheless, different areas under the *Pvs.d* curves are obtained, which correspond to the energy necessary to produce the respective discontinuity. The larger the discontinuity length, the more energy is needed to produce the discontinuity. The numerical solution with a SKON formulation corresponds to the solution for the discontinuity length $l_{d3}$ obtained with the KOS formulation, which is the case when the discontinuity was place at the centroid of the element, showing that the SKON may under or overestimate the energy as stated by [20].

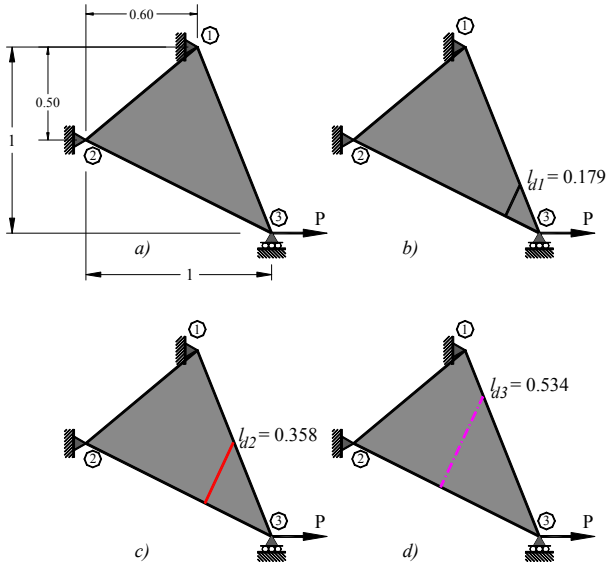


Fig. 5 Triangular element: a) geometric model, b) discontinuity $l_{d1}$, c) discontinuity $l_{d2}$ and d) discontinuity $l_{d3}$

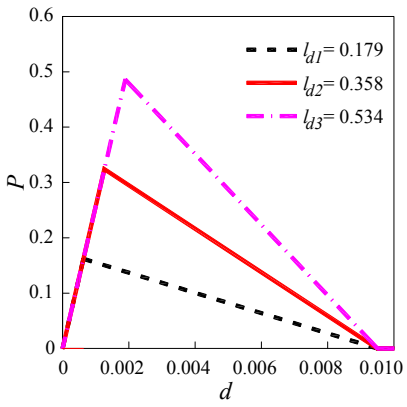


Fig. 6 Load *vs.* displacement curves

### B. Specimen Under Shear

The rectangular specimen with geometry and boundary conditions shown Fig. 7 is under a horizontal load applied at its upper part. Because the specimen is fixed from the base to the center of its height, shear stresses are localized along the longitudinal axis. The mechanical properties of the material were: Young´s modulus, *E=26.5MPa*, Poisson ratio *υ=0.3*, maximum shear stress, $\tau_u$=20 kPa and shear fracture energy density $G_{f1}$=*52.083 N/m*and$G_{f2}$ =*100N/m*. Plane strain was considered for the analysis.

Three different meshes with 2D triangular elements where used for the simulation of this specimen shown in Fig. 8; two of them were structured and the last one was unstructured. The computed load *vs.* displacement curves are congruent with the numerical results reported by [7], who applied a FEEDs of the SKON family. The areas under these curves, shown in Fig. 9, agree with the energy necessary to produce this discontinuity. It is interesting to say that [7] used a plasticity surface with softening, taking the ultimate shear stress as the yield stress.

This failure mode is considered as II, where the computed results were the same with both formulations, a fact attributed to that the total discontinuity length is the same and that the jump displacement is uniform.

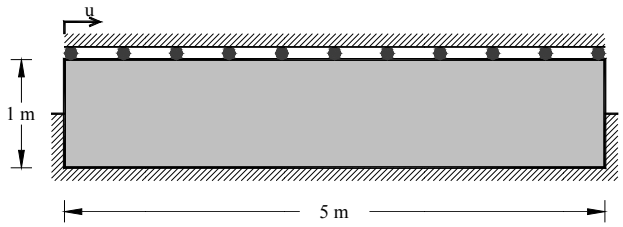


Fig. 7 Simple shear specimen

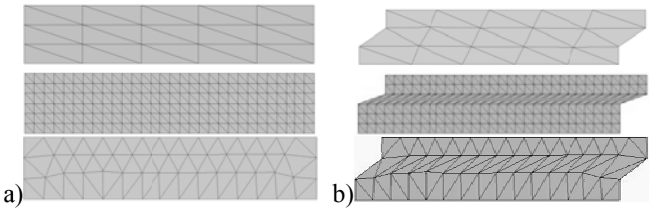


Fig. 8 Meshes: a) undeformed and b) damaged

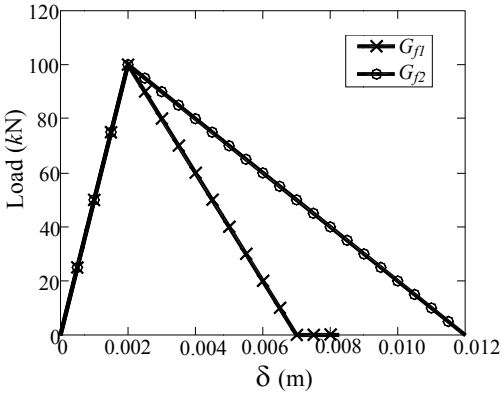


Fig. 9 Load *vs*. displacement curves

*C. Slopestability Problem*

A more complex example was developed by [19] and [25] using quadrilateral FEEDs of the KOS and SKON families, respectively. This is an embankment with a rigid footing placed on the crest, with dimensions and boundary conditions as shown in Fig. 10. In this paper, the embankment was discretized with triangular FEEDs as shown in Fig. 11 a. The mechanical properties of the soil were: Young´s modulus, *E=10 MPa*, Poisson ratio $\upsilon$*=0.45*, maximum tensile stress, $\sigma_u$*=100 kPa* and fracture energy density *Gf=80 MN/m*. In the analysis, a downward displacement is applied at the centre of the footing. Once the damage surface is reached, the material failure starts at the right lower corner of the footing, propagating along a curved path as shown in Fig. 11 b.

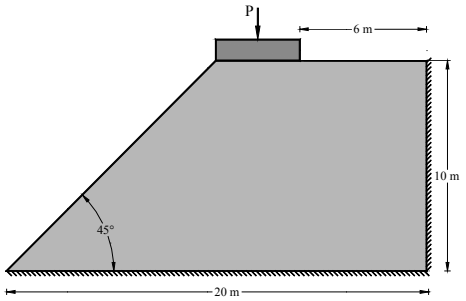


Fig. 10 Slope (adapted from [19])

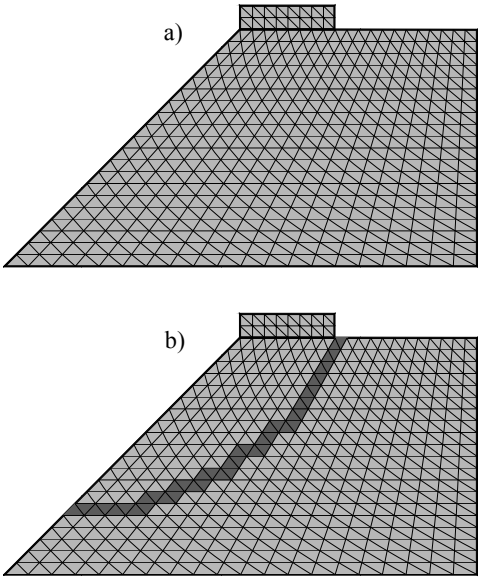


Fig. 11 Meshes: a) undeformed and b) localization zone

Fig. 12 shows the evolution of the load *P*, *vs.* the displacement δ, applied at the center of the footing. As can be seen, the numerical results reported by [25] show that the SKON formulation may overestimate the energy required to create the slip line, attributed to the fact that the SKON formulation does not include the length of the discontinuity as the proposed formulation. In reality, the total length of the discontinuity computed with the proposed formulation may be shorter than the computed with the SKON formulation.

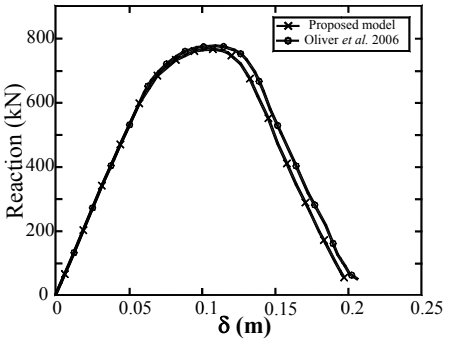


Fig. 12 Load *vs.* displacement curves

## VI. Conclusions

The triangular element with discontinuities non parallel to a border demonstrated that this formulation, member of the KOS family of FEEDs, does not induce spurious tractions when the discontinuity is placed in perpendicular direction to the principal stress.

In is shown that the SKON family may over or underestimate the energy required to create a discontinuity, as this effect is related with the total length of the discontinuity, fact that is not noticed when the discontinuity path is a straight line.

When the discontinuity length is considered into the analysis, the energy required to create a discontinuity may be less than with a SKON formulation, because this energy is directly related with the length of the path followed by the discontinuity.

## Acknowledgment

The first author thanks the support given by the Universidad Autónoma Metropolitana. The second and third authors thank the support given by the General Directorate of Academic Personnel affairs of the Universidad Nacional Autónoma de México.

## References

[1] J. Alfaiate, A. Simone, andL.J. Sluys,"Non-homogeneous displacement jumps in strong embedded discontinuities",*Int J Solids Struct*, vol. 40, no. 21, pp. 5799–5817, 2003.

[2] F. Armero, and K.Garikipati,"An analysis of strong discontinuities in multiplicative finite strain plasticity and their relation with the numerical simulation of strain localization in solids",*Int J Solids Struct,* vol. 33, no. 20-22, pp. 2863–2885, 1996.

[3] F. Armero, and C. Linder,"New finite elements with embedded strong discontinuities in the finite deformation range",*Comput Methods ApplMechEng*, vol. 197, no. 37-40, pp. 3138–3170, 2008.

[4] F. Armero, and C. Linder,"Finite elements with embedded branching"*Finite Elem Anal Des*,vol. 45, no. 4, pp. 280–293,2009.

[5] F. Armero, and D. Ehrlich,"Numerical modeling of softening hinges in thin Euler-Bernoulli beams", *Comp Struct*, vol. 84, no. 10-11, pp. 641–656,2006.

[6] F. Armero, and D. Ehrlich,"Finite element methods for the multi-scale modelling of softening hinge lines in plates at failure",*Comput Methods ApplMechEng*, vol.195, no. 13-16, pp.1283–1324, 2006b.

[7] R.Borja, "A Finite element model for strain localization analysis of strongly discontinuous field based on standard Galerkin approximation", *Comput Methods ApplMechEng*, vol. 190, pp. 1529–1549, 2000.

[8] L. Contrafatto, M. Cuomo, and G.T. Di Venti,"Finite elements with non-homogeneous embedded discontinuities",in*Proc.Eberhardsteiner J et. al. (Eds.), 6th European Congress on Computational Methods in Applied Sciences and Engineering, ECCOMAS*, Vienna - Austria, 2012, pp.1–20.

[9] L. Contrafatto, M. Cuomo, and F. Fazio,"An enriched finite element for crack opening and rebar slip in reinforced concrete members",*Int J Fracture*, vol. 178, no.1-2, pp. 33–50, 2012.

[10] D. Dias-da Costa, J. Alfaiate, L. Sluys, and E. Júlio,"Towards a generalization of a discrete strong discontinuity approach",*Comput Methods ApplMech*Eng, vol. 198, pp. 3670–3681, 2009.

[11] D. Dias-da-Costa, J. Alfaiate, LJ. Sluys, and E. Júlio,"A discrete strong discontinuity approach",*EngFractMech,* vol.76, no. 9, pp. 1176–1201,2009.

[12] J. Dujc, B. Brank, and A. Ibrahimbegovic,"Quadrilateral finite element with embedded strong discontinuity for failure analysis of solids",*CMES-Comp Model Eng*, vol. 69, no.3, pp. 223–260, 2010a.

[13] J. Dujc, B. Brank, A. Ibrahimbegovic, and D. Brancherie, "An embedded crack model for failure analysis of concrete solids", *Comput Concrete,* vol. 7, no.4, pp. 331–346, 2010b.

[14] J. Dujc, B. Brank, and A. Ibrahimbegovic, "Stress-hybrid quadrilateral finite element with embedded strong discontinuity for failure analysis of plane stress solids", *Int J Numer Meth Engng*, vol. 94, pp. 1075–1098,2013a.

[15] J. Dujc, B. Brank, and A. Ibrahimbegovic,"Embedded discontinuity finite element formulation for failure analysis of planar reinforced concrete beams and frames",*EngStruct*, vol. 50, pp. 115–125, 2013b.

[16] D. Ehrlich, and F. Armero,"Finite element methods for the analysis of softening plastic hinges in beams and frames", *ComputMech*, vol. 435, no. 4, pp. 237–264, 2005.

[17] A. E. Huespe, J. Oliver, P. J. Sanchez, S. Blanco, and V. Sonzogni,"Strong discontinuity approach in dynamic fracture simulations",*MecánicaComputacional*, vol. XXV, pp. 1997–2018, 2006.

[18] M. Jirásek, "Comparative study on finite elements with embedded discontinuities",*Comput Methods ApplMechEng*, vol. 188, no. 1-3, pp. 307–330, 2000.

[19] G. Juárez, and G. Ayala,"Variational formulation of the material failure process in solids by embedded discontinuities model",*Numer Methods Partial Differ Equ*, vol. 25, no. 1, pp. 26–62, 2009.

[20] G. Juárez-Luna, and G.A. Ayala, "Improvement of some features of finite elements with embedded discontinuities", *EngFractMech*, vol. 118, pp. 31–48, 2014.

[21] H. R. Lotfi, and P. Shing,"Embedded representation of fracture in concrete with mixed finite elements",*Int J Numer Methods Eng,* vol. 38, no. 8, pp. 1307–1325, 1995.

[22] J. Oliver,"Modelling strong discontinuities in solid mechanics via strain softening constitutive equations", Part 1: Fundamentals, vol. 39, no. 21, pp. 3575–3600, 1996. Part 2: Numerical simulation. *Int J Numer Methods Eng,* vol. 39, no. 21, pp. 3601–3623, 1996.

[23] J. Oliver, A. E. Huespe, M. D. G. Pulido, and E. Chaves,"From continuum mechanics to fracture mechanics: the strong discontinuity approach",*EngFractMech,* vol. 69, no. 2, pp. 113–136, 2002.

[24] J. Oliver, A. E. Huespe, and E. Samaniego, "A study on finite elements for capturing strong discontinuities",*Int J Numer Methods Eng*, vol. 56, no. 14, pp. 2135–2161, 2003.

[25] J. Oliver, A. E. Huespe, S. Blanco, and D. L. Linero,"Stability and robustness issues in numerical modeling of material failure with the strong discontinuity approach",*Comput Methods ApplMechEng*, vol. 195no. 52, pp. 7093–7114,2006.

[26] M. Ortiz, Y. Leroy, and A. Needleman,"A finite element method for localized failure analysis",*Comput Methods ApplMechEng*, vol. 61, no. 2, pp. 189–214, 1987.

[27] J. M. Sancho, J. Planas, DA. Cendón, E. Reyes, and J. C.Gálvez,"An embedded crack model for finite element analysis of concrete fracture", *EngFractMech*, vol. 74, no. 1-2, pp. 75–86, 2007.

[28] J. C. Simo, and J. Ju,"Strain and stress based continuum damage models, I. Formulation",*Int J Solids Struct*, vol. 23, no. 7, pp. 821–840, 1987.

[29] J. C. Simo, J. Oliver, and F. Armero, "An analysis of strong discontinuities induced by strain-softening in rate-independent inelastic solids", *ComputMech*, vol. 12, no. 5, pp. 277–296, 1993.

[30] J. C. Simo, and J. Oliver, "A new approach to the analysis and simulation of strain softening in solids",in *Proc*: *Bazant ZP et. al. (Eds.)*, *Fracture and Damage in Quasibrittle Structures*, *E. and F.N. Spon*, London, 1994, pp. 25–39.

[31] G. N. Wells,and L. J. Sluys, "A new method for modelling cohesive cracks using finite elements"*Int J Numer Methods Eng*, vol. 50, no. 12, pp. 2667–2682, 2001.